Study on the Technique of Ellipse Excavation and Tilt Correction of the Stone Statues of the Northern Song Dynasty Imperial Mausoleum

Qingwen Ma (Mqw2008@zzu.edu.cn)
Zhengzhou University https://orcid.org/0000-0002-5924-2691
yangyang wang
Zhengzhou University
Sihan Liu
Zhengzhou University
Xinyu Fan
Zhengzhou University

Research Article

Keywords: Stone statue, Oval cut hole, Numerical Analysis, Digging soil correction test

Posted Date: June 1st, 2021

DOI: https://doi.org/10.21203/rs.3.rs-525159/v1

Study on the technique of ellipse excavation and tilt correction of the stone statues of the Northern Song Dynasty imperial mausoleum

Qingwen Ma [1], Yangyang Wang [1], Sihan Liu [1], Xinyu Fan [1]

[1]School of Water Conservancy Science and Engineering, Zhengzhou University, Zhengzhou450001, P. R. China

Mqw2008@zzu.edu.cn

Abstract: This article takes the stone statues of the Northern Song Dynasty imperial mausoleum as the research object. Aiming at the characteristics of the stone statues low weight and small building area, combined with the serious weathering of the stone statues, the reasons for the inclination and the defects of the traditional round soil excavation holes, an elliptical soil excavation correction method is proposed. Adopt the method of combining numerical simulation and experiment to carry out the research of elliptical excavation and tilt correction of stone statues. Research indicates: The settlement difference between the excavation side and the non-excavation side increases with the increase of the span-to-height ratio of the excavation hole; The shallower the depth of the digging hole, the greater the settlement difference between the digging side and the non-digging side; The settlement difference between the digging side and the non-digging side decreases with the increase of the hole spacing; The settlement of the superstructure mainly occurs within 4 to 5 hours after the soil is excavated, and then enters a slow growth stage, and finally gradually stabilizes; During the test, the failure of the digging hole belongs to plastic failure. The damage of the digging hole is firstly destroyed from both sides of the hole, and the upper part of the hole is destroyed immediately, and the upper structure edge is destroyed first.

Key words: Stone statue; Oval cut hole; Numerical Analysis; Digging soil correction test

1.Introduction

Tomb stone carvings, also known as "Stone Statues", are one of the main elements of the tomb[1]. At present, the surviving stone statues have caused various diseases due to natural erosion and man-made destruction. Among them, the tilt of the stone statues is one of the most important diseases affecting its overall stability. There are many research results in the field of tilt correction technology for existing buildings at home and abroad. Terracina[2] first proposed the idea of rectifying tilt to relieve the stress of the building foundation in the plan to save the Leaning Tower of Pisa. Tugaenko [3] successfully corrected the tilt of a 16-story residential building by using the flooding method. Green[4] studied the influence of multiple circular excavation holes with different diameters on the stress distribution of the foundation

under different spatial conditions. Liu Zude[5] put forward the technique of rectification and reinforcement of foundation stress relief method. Qin Shanglin[6] used an engineering example in which a 6-story comprehensive building was seriously inclined due to the existence of a weak soil layer underneath the foundation, and proposed a combination of horizontal excavation and grouting reinforcement to correct inclination and reinforcement.Zhu Yanpeng[7] proposed an expansion correction method for inclined buildings in collapsible loess areas, and derives the calculation formula for the amount of expansion material with the aid of the pore compaction principle.Zhang Xuqiang[8] took the Elephant Temple Pagoda in Heyang, Shaanxi as the research object, and analyzed the relationship between the water content of loess and the amount of compression combined with the indoor compression test.Cheng Xiaowei[9] used the method of soil excavation combined with anchor cable pressure to correct the inclination of a high-rise residential building.At present, shallow excavation and forced landing in tilt correction projects often rely on experience to correct tilt, and most of the earth excavation holes are round earth excavation holes. However, when the upper load is small and the building area is small, it is often difficult to achieve the expected tilt correction goal for the circular soil excavation hole. If the size of the soil excavation hole is too small, the correction will be very slow and the effect is not ideal. Excessive tilt correction caused the upper building to tilt in the opposite direction.Aiming at the above problems, this paper proposes an elliptical soil excavation correction method.By changing the ratio of the long and short axis of the elliptical soil excavation hole, the stress concentration coefficient of the soil around the excavation hole is controlled, so that the base soil is more susceptible to disturbance under low loads. Compression deformation occurs.

2.The mechanism of elliptical correction and the analysis of instability

2.1 The mechanism of elliptical excavation and tilt correction

The elliptical digging and tilting correction of the stone statue refers to the special design, by extracting a part of the soil from a certain depth of the soil under the foundation of the stone statue, forming a specific size, direction, depth and spatial distribution (single row or multiple rows) The elliptical hole reduces the pressure-bearing area of the foundation soil, so that the contact stress slowly increases, which promotes the collapse of the excavation hole, resulting in settlement of the upper foundation surface, forcing the foundation to sink, and causing the stone statue body to follow the established trajectory. The "rigid body" rotates to adjust the uneven settlement and achieve the purpose of tilt correction, which belongs to the digging and forced landing of tilt correction [10]. A schematic diagram of digging soil to correct tilt, as shown in Figure 1.

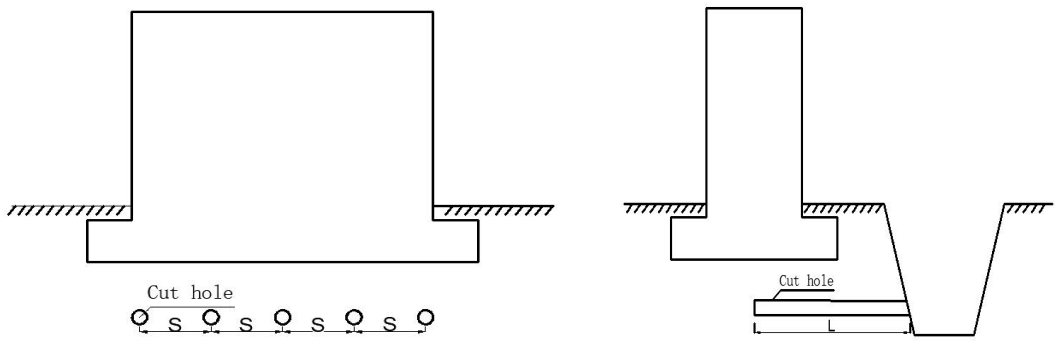

（a）Schematic diagram of elevation （b）Schematic diagram of cross-section

Figure 1 Schematic diagram of soil excavation and tilt correction

2.2 Analytical formula for the stress around the hole of the elliptical digging hole

Suppose the cross-section of the elliptical digging hole is the z-plane, and the z-plane has an elliptical digging hole with a semi-major axis a and a semi-minor axis b. The coordinate system is established with the center o of the digging hole as the origin 2 show.

First, conformal transformation is used to turn the boundary of the non-circular hole into a circular boundary, and the analytical solution obtained on the circular boundary is changed back, so that the solution of the original problem can be obtained. The conformal mapping function [11] is:

$$z = \omega(\xi) = n\left(\xi + \frac{m}{\xi}\right) \tag{1}$$

In the formula:n=(a+b)/2； m=(a-b)/(a+b)。

The elliptical digging hole in the z-plane is mapped to the unit circle with a plane radius of 1 as shown in Figure 3. After transformation, the stress expression of the elliptical digging hole can be derived as:

$$\sigma_\theta = \lambda P \frac{1 - 2\cos 2\theta - m^2 + 2m}{1 - 2m\cos 2\theta + m^2} + P \frac{1 + 2\cos 2\theta - m^2 - 2m}{1 - 2m\cos 2\theta + m^2} \tag{2}$$

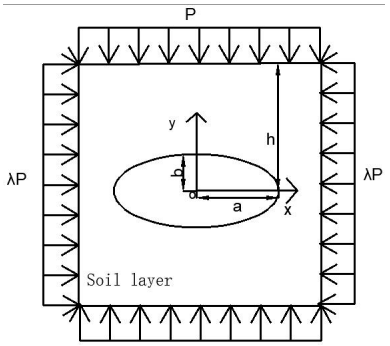

Figure 2 Stress calculation model of an elliptical orifice on the z-plane

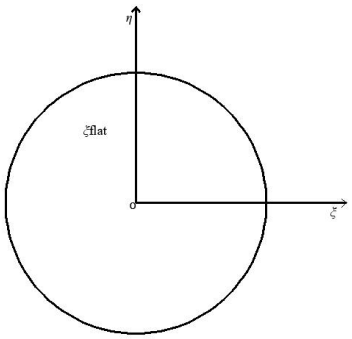

Figure 3 The unit circle with radius 1 on the ξ plane

2.3 Judgment criteria for the failure of the elliptical cut hole

In this paper, the method of combining stress component expression and stress

coordinates is used to obtain the maximum and minimum principal stresses at the edge of the elliptical excavation hole, and the Mohr-Coulomb strength failure criterion is used to determine whether the excavation hole will fail.

(1) Stress coordinate conversion and principal stress solution

The transformation relation of stress components from polar coordinates to rectangular coordinates is:

$$\begin{cases} \sigma_x = \sigma_\rho \cos^2\theta + \sigma_\theta \sin^2\theta - 2\tau_{\rho\theta}\sin\theta\cos\theta \\ \sigma_y = \sigma_\rho \sin^2\theta + \sigma_\theta \cos^2\theta + 2\tau_{\rho\theta}\sin\theta\cos\theta \\ \tau_{xy} = (\sigma_\rho - \sigma_\theta)\sin\theta\cos\theta + \tau_{\rho\theta}(\cos^2\theta - \sin^2\theta) \end{cases} \quad (3)$$

$$\begin{cases} \sigma_{\max} = \dfrac{\sigma_x + \sigma_y}{2} + \sqrt{\left(\dfrac{\sigma_x - \sigma_y}{2}\right)^2 + \tau_{xy}^2} \\ \sigma_{\min} = \dfrac{\sigma_x + \sigma_y}{2} - \sqrt{\left(\dfrac{\sigma_x - \sigma_y}{2}\right)^2 + \tau_{xy}^2} \end{cases} \quad (4)$$

(2) Mohr-Coulomb strength criterion judgment

According to the geometric relationship between the shear strength line of the soil and the stress Mohr circle, the limit equilibrium condition of the soil is established[12]:

$$\sigma_1 = \sigma_3 \tan^2\left(\frac{\pi}{4} + \frac{\varphi}{2}\right) + 2c\tan\left(\frac{\pi}{4} + \frac{\varphi}{2}\right) \quad (5)$$

In the formula: σ_1 is the maximum principal stress; σ_3 is the minimum principal stress; c is the cohesive force; φ is the angle of internal friction.

From equation(4), σmin can be obtained, and $\sigma_{min}=\sigma_3$ is substituted into equation(5) to obtain σ_1. If $\sigma_{max}>\sigma_1$, the excavation hole starts to fail at this point.

2.4 Instability analysis of the failure of the elliptical cut hole

Based on the principle of load symmetry, this paper will select 1/4 soil excavation holes at 15° intervals in the counterclockwise direction on the z-plane to divide, as shown in Figure 4. Use equations (2) and (3) and use matlab to calculate the stress values of 7 key points on the sides of the soil hole a~g, and then make judgments based on the soil limit equilibrium condition equation (5).

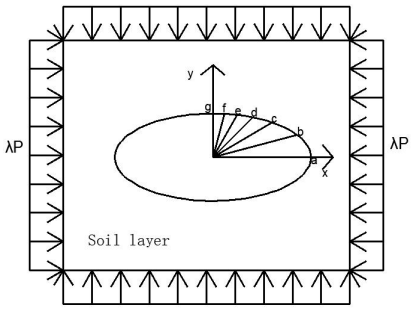

Figure4 The edge of the 1/4 elliptical digging hole is divided at 15° intervals

2.4.1 Calculation model and evaluation index

The values of relevant parameters in the calculation model are shown in Table1.

Table 1 Parameter values

parameter	φ/(°)	c/KPa	E/MPa	μ	λ	$P/(g\cdot cm^{-3})$	$P/$（KPa）
Numerical	20	28	23.20	0.25	0.50	1.45	70

In this paper, the ratio of the principal stress value σ_1 of the soil under the limit equilibrium state to the maximum stress value σ_{max} around the digging hole is used to judge the stability of the digging hole [13], and the stability coefficient k is introduced:

$$k = \sigma_1 / \sigma_{\max} \quad (6)$$

When the stability coefficient k<1, it indicates that the elliptical digging hole is unstable, that is, the digging hole is easy to deform, which can effectively disturb the foundation soil and cause foundation settlement. If the stability coefficient k≥1, it indicates that the elliptical digging hole is stable, the digging hole will not be deformed, and the tilt correction project will appear "digging without tipping", and auxiliary measures need to be taken to promote the damage of the digging hole .

2.4.2 Analysis of the influence of the ratio of the long and short axis of the cut hole on the stability

It can be seen from formula(2) that the influence of the ratio of the long and short axis of the excavation hole on the stability of the excavation hole is realized by the parameter m, which can be known from the expression of the parameter m (m=1 － 2b/(a+b)), When the short axis b of the excavation hole remains unchanged, m is positively correlated with the long axis a of the excavation hole. In this paper, in order to analyze the influence of the ratio of the length and the short axis of the elliptical digging hole on the stability of the digging hole, four elliptical digging holes with different ratios of the length and the short axis are designed: 1:1, 1:1.5, 1:2 , 1:2.5. Make the short axis b=80mm of the soil cutting hole unchanged, and take the long axis a 80mm, 120mm, 160mm, 200mm. It also calculates the maximum and minimum stress values of 7 key points at the edge of the soil-excavating hole a~g when the upper load is 70KPa. The settlement result is shown in Table 2.

Table 2 Stress value of the hole edge of the soil cutting hole/KPa

Long and short axis ratio	stress	key point						
		a	b	c	d	e	f	g
1：1	σ_{min}	0.00	0.00	0.00	0.00	0.00	0.00	0.00
	σ_{max}	175.00	165.62	140.00	105.00	70.00	44.38	35.00
1：1.5	σ_{min}	0.00	0.00	0.00	0.00	0.00	0.00	0.00
	σ_{max}	245.00	212.55	145.00	83.46	41.77	18.88	11.67
1：2	σ_{min}	0.00	0.00	0.00	0.00	0.00	0.00	0.00
	σ_{max}	315.00	244.72	135.00	63.00	24.23	5.55	0.00
1：2.5	σ_{min}	0.00	0.00	0.00	0.00	0.00	-2.55	-7.00
	σ_{max}	385.00	263.58	120.14	47.07	12.85	0.00	0.00

It can be seen from Table 2 that when the upper load is 70KPa, the elliptical excavation hole has the largest stress at point a, that is, this point has the least stability and is most prone to damage. The stress at point a increases as the ratio of the long and short axis of the excavation hole increases, and when the ratio of the long and short axis of the elliptical excavation hole is 1:2.5, tensile stress appears at the two points f and g of the excavation hole.

In order to more intuitively describe the influence of the ratio of the length of the elliptical digging hole on the stability of the digging hole, the stability coefficients of the elliptical digging hole under four working conditions are further calculated, and the settlement results are shown in Figure 5.

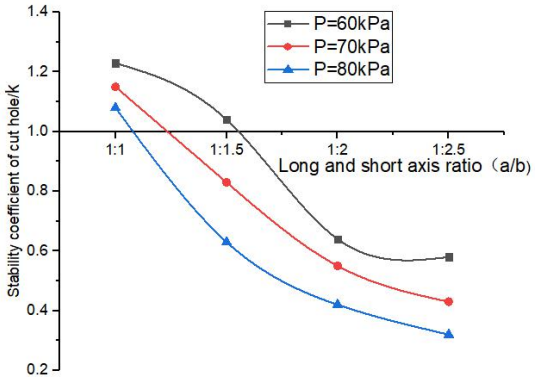

Figure 5 The relationship curve between the ratio of the long and short axis of the cut hole and the stability coefficient of the cut hole

It can be seen from Figure 5 that the stability of the digging hole is inversely proportional to the ratio of the long and short axis of the elliptical digging hole. Especially when the ratio of the long and short axis is 1:1, that is, when m=0, the elliptical digging hole degenerates into a circular digging hole. At this time, the stability coefficient of the digging hole is the largest, and it is not easy for the digging hole to be in a stable state damage. Therefore, when the upper load is small, the elliptical digging hole is more prone to instability and deformation than the circular digging hole, which can effectively disturb the foundation soil and cause foundation settlement.

3 Analysis of the influencing factors of the elliptical digging soil correction method

3.1 Establishment of finite element model

Taking the Yongchang Tomb West Military Attaché stone statue as an example, a simplified modeling was carried out based on the site survey results. The overall size of the numerical simulation soil model is 2m×2m×2m, and the plane size of the stone cushion is 0.7m×0.7m. The effect of the soil excavation process on the stone body is not considered, and the load of the stone body is replaced by a uniform load. The body weight of the West Military Officer's stone statue is 2 tons, that is, the load on the upper part of the model soil is 57142N/㎡. The overall grid size is 0.08m, and the soil excavation hole area is encrypted, as shown in Figure 6.

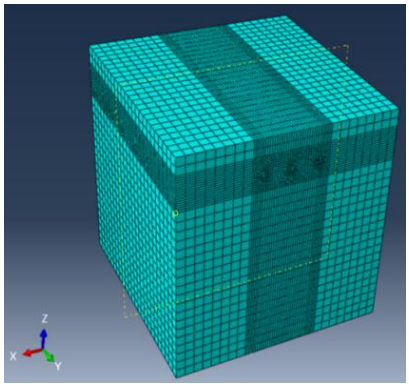

Figure 6 Overall grid model diagram

The top of the model is a free boundary, and the bottom is a fixed boundary. The lateral soil is constrained in the X and Y directions respectively. According to the geological survey report, the basic parameters of the foundation soil are shown in Table 3. A total of 6 settlement monitoring points are selected on the calculation model, of which 3 are on the south side and 3 are on the north side. The selection of monitoring points should avoid selecting corner points, because corner points are prone to stress concentration and excessive displacement.

Table 3 Simulated soil parameters

parameter	φ/(°)	c/KPa	E/MPa	μ	λ	P/($g \cdot cm^{-3}$)
Numerical value	20.00	18.00	23.20	0.25	0.50	1.45

3.2 Analysis of simulation results

3.2.1 Settlement analysis under different burial depth influencing factors

Set the size of the elliptical excavation hole: short axis b=80mm, long axis a=140mm, hole spacing 250mm, and excavation depth 1000mm; the buried depth h of the excavation hole is 200mm, 300mm, 400mm and 500mm. Analyze the situation. The settlement of the foundation soil under different hole buried depth conditions is shown in Figure 7~8.

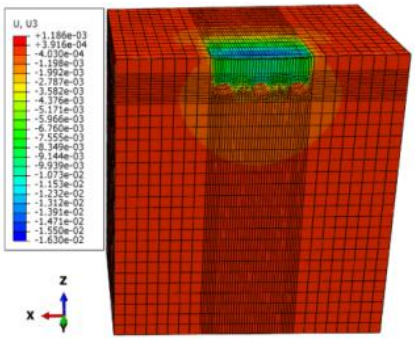

Figure7 Hole depth/200mm

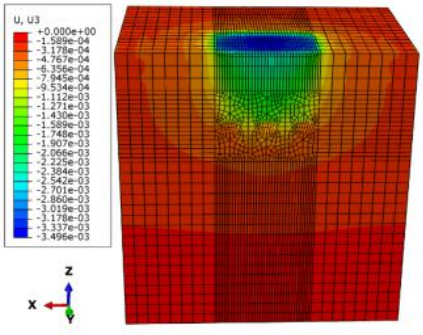

Figure8 Hole depth/500mm

As shown in Figure 9: the settlement of each measuring point decreases as the depth of the excavation hole increases. When the burial depth of the digging hole is 400mm, the settlement value of each measuring point is small, the maximum value appears at measuring

point 2, and the settlement is 3.48mm. When the burial depth of the digging hole is less than 400mm, the settlement of each measuring point on the side of the digging hole Rapid increase, and when the burial depth of the excavation hole is greater than 400mm, the settlement of each measuring point decreases slowly. It can be seen from Figure 10 that when the buried depth of the excavation hole is 200mm, the north-south settlement difference is 7.523mm, and the tilt correction effect is more obvious. When the buried depth of the excavation hole is 500mm, the north-south settlement difference is 1.780mm, and the tilt correction effect is not obvious.

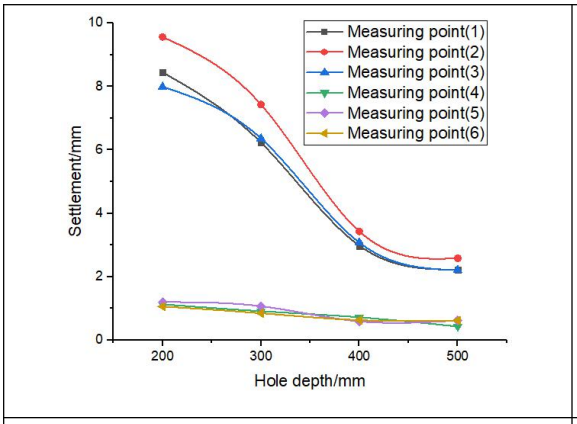

Figure9 Settlement value of each measuring point varying with hole depth

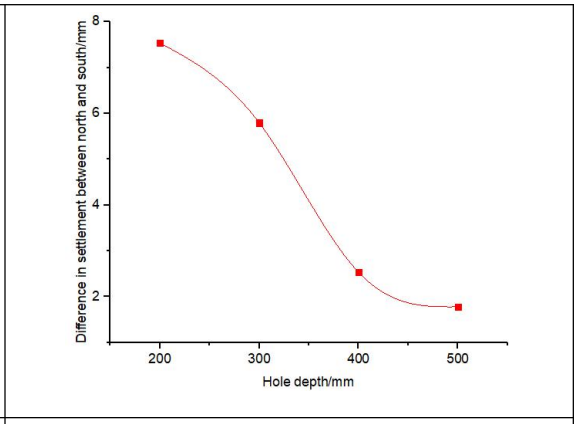

Figure 10 The difference in settlement between north and south under different borehole depth conditions

3.2.2 Settlement analysis under the influence factors of different hole spacing

Set the size of the elliptical digging hole as short axis b=80mm, long axis a=120mm, burial depth of the digging hole 300mm, and digging depth 1000mm; the spacing s of the digging hole is 180mm, 200mm, 220mm, 240mm, 260mm and 280mm. The settlement of the foundation soil under different hole spacing conditions is shown in Figures 11-12.

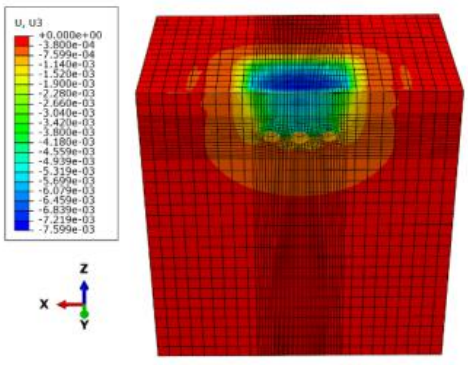

Figure 11 Hole spacing/180mm

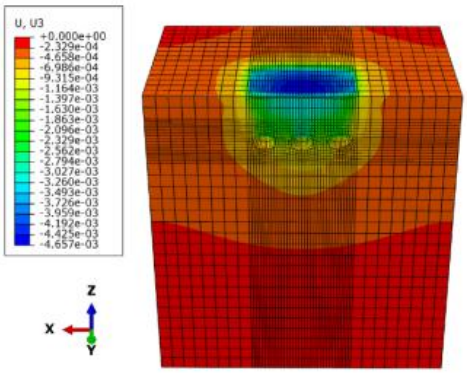

Figure 12 Hole spacing/240mm

It can be seen from Figure 13 that the settlement of each measuring point decreases with the increase of the soil excavation hole spacing, and the settlement of each measurement point on the north side (the soil excavation side) decreases linearly with the increase of the hole

spacing, and the south side (The non-excavation side) the settlement of each measuring point is relatively stable. It can be seen from Figure 14 that when the distance between the excavation holes is reduced from 280mm to 180mm, the north-south settlement difference of the foundation soil increases from 1.823mm to 5.231mm. This is because when the distance between the excavation holes is reduced, the two adjacent excavation holes The plastic zones around the hole overlap each other, which accelerates the deformation and stress redistribution of the foundation soil

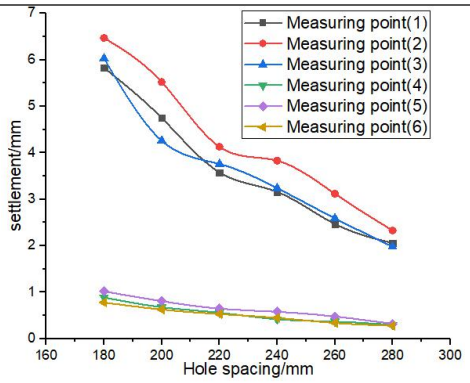

Figure 13 Settlement value of each measuring point with the change of hole spacing

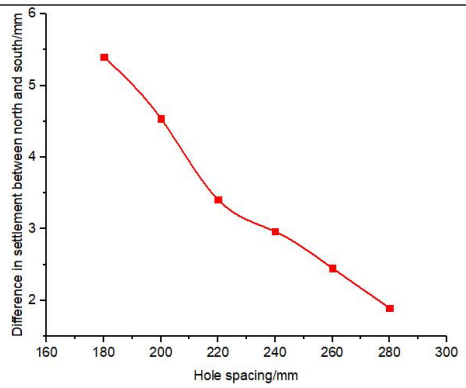

Figure 14 The difference in settlement between north and south under different hole spacing conditions

3.2.3 Settlement analysis under different influencing factors of soil cut hole size

In order to analyze the influence of the size of the elliptical digging hole on the tilt correction effect, firstly define the parameter n=a/b, where a is the long axis of the elliptical digging hole and b is the short axis of the elliptical digging hole, that is, the parameter n is the elliptical The span-to-height ratio of the soil holes is designed to be 250mm, the buried depth of the soil holes is 300mm, the soil depth is 1000mm, b=80mm is fixed, a is 100mm, 120mm, 140mm, 160mm, 180mm and 200mm respectively n is 1.25, 1.5, 1.75, 2, 2.25, 2.5 six working conditions for analysis.

The settlement of foundation soil under different span-to-height ratios of cutout holes is shown in Figures 15-16.

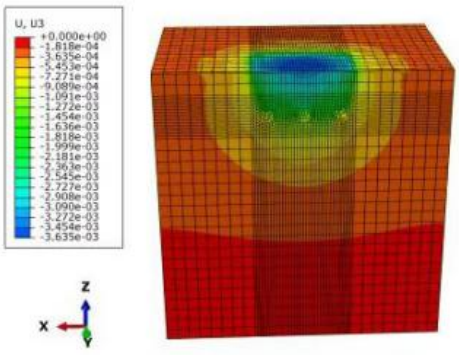

Figure 15Long axis/ a=100mm

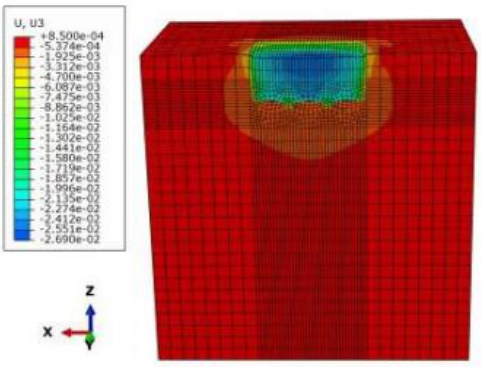

Figure 16 Long axis/a=200mm

It can be seen from Figure 17 that the settlement of each measuring point on the north side (the side of the soil excavation) increases with the increase of the span-to-height ratio of the soil excavation hole, and the settlement of point 2 is the largest. In the interval between 1.75 and 2.5, the increase rate of settlement at each measuring point is the fastest. Although the settlement of each measuring point on the south side (non-excavation side) increases with the increase of the span-to-height ratio of the excavation hole, the amount of change is small. It can be seen from Figure 18 that the north-south settlement difference of the foundation soil increases with the increase of the span-to-height ratio of the excavation hole, but the growth rate is different. When the span-to-height ratio n of the cut hole increases from 1.25 to 1.75, the north-south settlement difference increases from 2.665mm to 5.793mm, an increase of about 117%; n increases from 1.75 to 2.5, the north-south settlement difference increases from 5.793mm to 22.953mm, an increase That's about 296%.

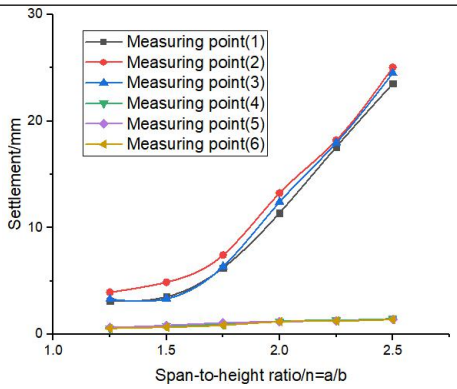

Figure 17 Settlement of each measuring point with the change of the ratio of the span to the height

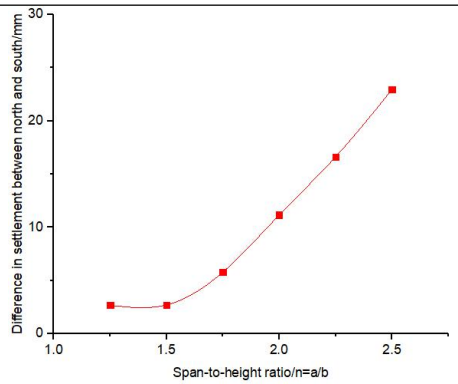

Figure 18 Difference in settlement between north and south under different span-to-height ratios

4 Experimental study on elliptical excavation of stone statues

4.1 Experimental design

In order to meet the needs of the test, a geotechnical model box was specially designed and produced with a size of 1000mm×1000mm×1200mm. The side plate of the model box on the side of the hole is connected by bolts to the steel plate and square steel, so that it can be easily disassembled manually when digging out the soil. The steel plate realizes the function of digging out soil. The model box is shown in Figure 19a. The soil used for the experiment was taken from the place where the stone statue of the West Military Attaché in Yongchang Tomb was born.

（a）Model box

（b）The box is filled with soil

Figure 19 The entity of the geotechnical test model box

Table 4 Basic parameters of model soil

Parameter	φ/(°)	c/KPa	E/MPa	μ	λ	P/($g \cdot cm^{-3}$)
Number	20.00	18.00	21.80	0.25	0.50	1.45

In order to ensure that the model soil is similar in weight and compaction to the bottom soil layer of the original inclined building, the model soil should be compacted in layers, manually ramming once every 200mm of the filled soil in the model box, and the sinking of each layer of model soil is 50mm as the compaction standard . In order to ensure that the weight of the model soil remains the same, the model soil samples are taken to measure the weight and compaction of each 300mm increase in the filling of the model box, so as to adjust the compaction process in time. The soil weight in the model box is determined to be 18KN/m³, and the compaction coefficient is 0.905. The completed model soil rammed soil is shown in Figure 19b.

4.2 Test loading and measurement plan

The test adopts the jacking method to load. A steel backing plate with a size of 700mm×500mm×15mm is made of I-beam instead of the stone lining and placed on the surface of the model soil; the distribution beam is 250mm×250mm×9mm×14mm I-beam with a length of 500mm; hydraulic jacks are used The height is 280mm, the running diameter is 100mm, and the maximum lifting force is 5t. Use No. 10 channel steel to make a simple reaction frame that meets the test loading requirements. When pressurized to 2 tons at a time, a uniform load of 57142N/㎡ can be obtained.

In order to obtain detailed changes in the settlement of the superstructure during the excavation process and after the excavation is completed, two electronic digital dial indicators are fixed on the steel backing plate to observe the vertical settlement of the superstructure. In the early stage of settlement, the change is large, and the data is recorded every 0.3h, while the later settlement change is small, and the data is recorded every 1h.

4.3 Design of elliptical soil excavation and tilt correction conditions

Set the burial depth of the excavation hole to 300mm, the hole spacing to 250mm, the

excavation depth to 500mm, the short axis of the oval excavation hole b=80mm, the upper load to 2 tons, and the upper structure area to be 0.7m×0.5m. Details The parameter design of working conditions is shown in Table 5.

Table 5 Working condition table of cut hole design

Working condition	Span-to-height ratio/$n=a/b$	Clear distance between holes s/mm	a/mm
1	1.75	110	140
2	2.00	90	160
3	2.25	70	180
4	2.50	50	200

Take working condition 1 as an example, the soil excavation process is the same for other working conditions. First, use a jack with a pressure gauge to pressurize to the design load at a time. When the data of the electronic digital dial indicator is stable, reset it to zero, and then carry out the soil excavation test. Hole digging is divided into two stages: centering the hole and digging the soil to form the hole.

Step 1: centering the hole

First, suppose that the position of the excavation hole is quantitative, that is, the influence of the tilt of the excavation hole on the tilt correction effect caused by artificial excavation is not considered, and the height of the excavation hole center from the base is 300mm. According to the design of the test conditions, the long axis of the excavation hole a=140mm, the short axis b=80mm, and the hole spacing 250mm. The center of the excavation hole from left to right is A, B, C, and the center of each circle reaches the model. The distance on the left side of the box is 250mm, 500mm, and 750mm. The center layout of the soil cutting hole is shown in Figure 20.

Step 2: Dig the soil

After the location of the hole center of the soil excavation hole is determined, a Luoyang shovel is used to manually excavate the soil. Digging should be carried out in phases and batches to avoid sudden sinking due to rapid or uneven digging. The sequence of digging holes is hole A, hole C, and hole B. The completed drawing of soil cutting is shown in Figure 21.

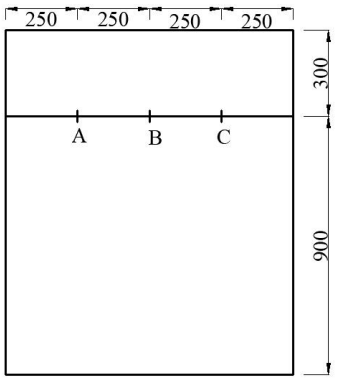

Figure 20 Layout of soil cut holes

Figure 21 Completed drawing of soil cutting

4.4 Test results and analysis

4.4.1 Settlement analysis of working condition 1 (span-height ratio of soil excavation hole n=1.75)

It can be seen from Fig. 22 that the settlement of the superstructure changes rapidly at first, and then enters a stage of slow change, and finally the settlement gradually stabilizes. The entire excavation work took 1.1 hours. Before the excavation work was completed, the settlement of the superstructure was small. The settlement changes mainly occurred after the excavation work was completed, and the superstructure was between 1.1h and 5.5h. The settlement of the slab is linearly changed. After 5.5h, the settlement changes steadily and gradually stays in a stable state, and the settlement difference between monitoring point 1 and monitoring point 2 gradually increases, and the upper structure begins to gradually tilt toward the side of soil excavation. The final settlement of monitoring point 1 (the side of the excavation) is 5.623mm, the settlement of monitoring point 2 (the side of the non-excavation) is 1.088mm, and the settlement difference between the side of the excavation and the non-excavation is 4.535mm.

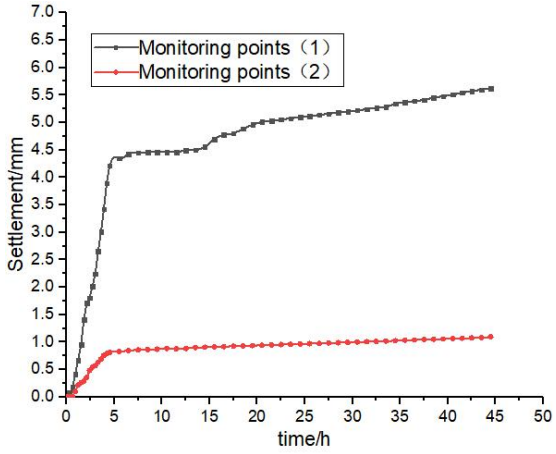

Figure 22. Settlement curve of superstructure in working condition 1 versus time

4.4.2 Settlement analysis of working condition two (span-height ratio of soil excavation hole n=2)

It can be seen from Figure 23. At 1.5h, the excavation work ends, and the settlement of monitoring point 1 (the excavation side) is 1.658mm at this time. The settlement of the superstructure mainly occurs within 5h after the end of the soil excavation. The settlement of the No. 1 monitoring point at this stage is 66.3% of the final settlement. After 6.5h, the settlement of the superstructure changes slowly and gradually stabilizes. From the change in settlement of monitoring point 2 (non-excavation side), it can be seen that there is also a certain amount of settlement on the non-excavation side. This is because the artificial rammed soil is not dense and the soil has a small amount of settlement under the upper load. The final settlement of monitoring point 1 (excavation side) is 10.575mm, the final settlement of

monitoring point 2 (non-excavation side) is 1.098mm, and the settlement difference between the excavation side and the non-excavation side is 9.477mm.

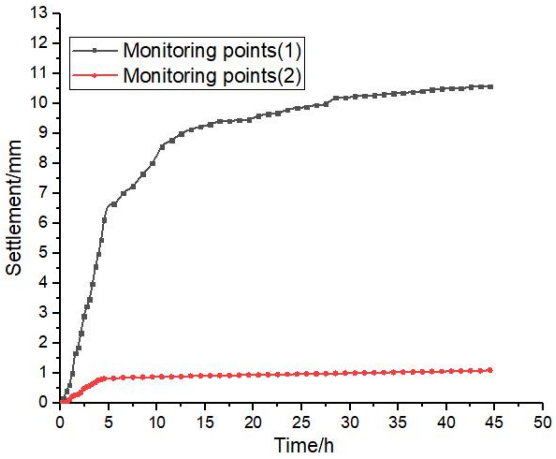

Figure 23 Settlement curve of superstructure in working condition 2 versus time

4.4.3 Settlement analysis of working condition 3 (span-height ratio of soil excavation hole n=2.25)

Figure 24 shows the change curve of the settlement of the superstructure with time under the design conditions of working condition 3. At 1.8h, the excavation work was completed. At this time, the settlement of monitoring point 1 (the excavation side) was 8.011mm, which was about 49.2% of the total settlement. The settlement changes of the superstructure are mainly concentrated in the two time periods of 1.2h~4.5h and 8.5h~18.5h. It can be seen from Figure 19 that the settlement of the superstructure increases linearly between 1.2h and 4.5h, the settlement of the superstructure changes slowly between 4.5h and 8.5h, and the settlement of the superstructure between 8.5h and 18.5h It exhibits a parabolic growth, and the settlement change of the superstructure between 18.5h and 45.5h is relatively stable and gradually stabilizes. The final settlement of monitoring point 1 (the side of the digging) is 16.280mm, the settlement of monitoring point 2 (the side of the digging) is 1.202mm, and the settlement difference between the side of the digging and non-digging is 15.078mm.

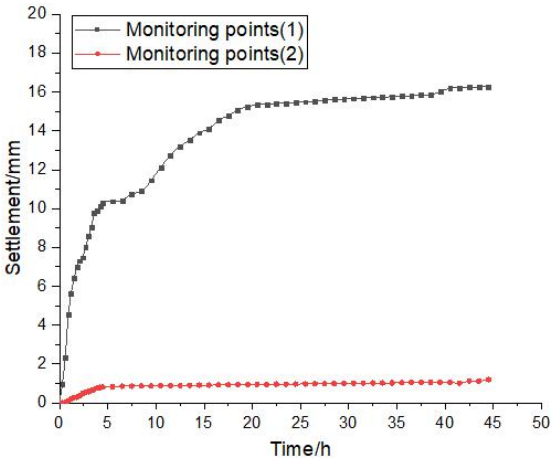

Figure24 Settlement curve of superstructure in working condition 3 versus time

4.4.4 Settlement analysis of working condition 4 (span-height ratio of soil excavation hole n=2.5)

Figure 25 shows the change curve of the settlement of the superstructure with time under the design conditions of working condition 4. At 2.1h, the excavation work was completed. At this time, the settlement of monitoring point 1 (the excavation side) was 9.797mm, which was about 43.9% of the total settlement. It can be seen from the graph that the settlement of the upper structure between 0.6h and 18.5h exhibits a parabolic increase, and the change of the settlement of the upper structure between 18.5h and 45.5h is relatively stable and gradually stabilizes. The final settlement of monitoring point 1 (excavation side) is 22.287mm, the settlement of monitoring point 2 (non-excavation side) is 1.203mm, and the settlement difference between the excavation side and the non-excavation side is 21.084mm.

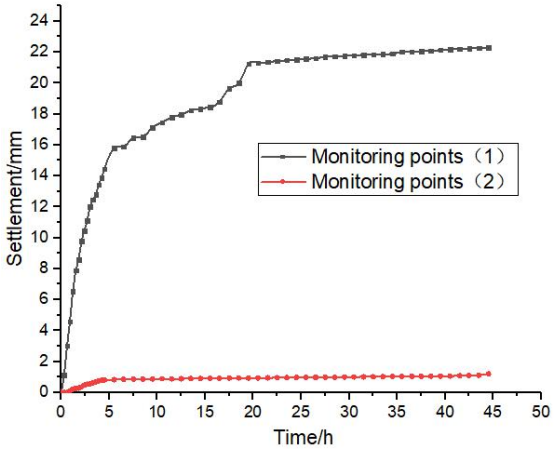

Figure25 Settlement curve of superstructure in working condition 4 versus time

4.4.5 Analysis of Deformation of Digging Hole

Due to the small size of the excavation hole in the working condition 1, the clear distance between the holes is large, and the soil strips between the excavation holes form a stable soil arch, that is, there is no obvious around the excavation hole during the entire excavation test process. The digging hole remains the same as the shape when the digging is completed, as shown in Figure 26.

Figure 26: Working condition one, the state of the earth-cut hole

By observing the deformation of the soil cutting hole in the second working condition, it can be seen that after the soil cutting hole A and the soil cutting hole C are completed, because the distance between the two holes is too large and the amount of soil is small, the soil cutting hole does not collapse. Appears, the A cutting hole is accompanied by the B

cutting hole, and the A cutting hole is slightly falling on the right side at a distance of 300mm from the hole, as shown in Figure 27. When the second working condition is completed, as time goes by, the B-cut hole is about 250mm away from the hole, that is, there are obvious signs of collapse at the edge of the steel backing plate made of I-shaped steel, such as Shown in Figure 28.

Figure 27 The surface state of the second cut hole A in the working condition

Figure. 28 Surface state of hole B in working conditio2

By observing the deformation of the soil-cutting hole in the three-digging process under working conditions, it can be known that when the soil-cutting work of the soil-cutting hole A and the soil-cutting hole C is completed, the stress around the hole cannot reach the failure condition, and the shape of the soil-cutting hole is stable. When the excavation of hole B is completed, the net distance between two adjacent holes is reduced, and the soil stress is redistributed under the action of the upper load, stress concentration occurs around the excavation hole, and the excavation hole has different degrees of deformation. A large amount of falling soil appears on the sidewall of the soil hole, as shown in Figure 29. B. Digging hole is about 250mm away from the orifice, that is, at the edge of the steel backing plate made of I-shaped steel. Compared with the condition 3, the collapse hole range is obviously enlarged, and the whole piece of soil collapse appears, as shown in Figure 30.Show.

Figure29 Surface state of three soil holes A under working condition

Figure30 Surface state of three soil holes B under working condition

By observing the deformation of the cutting hole in the process of working condition 4,

it can be seen that: compared with the first three working conditions, the size of the cutting hole and the amount of cutting are greatly increased, and the net distance between holes is also reduced from 110mm to 50mm. . When the excavation work of soil excavation hole A and soil excavation hole C is completed, the hole spacing between hole A and C is relatively large, the amount of inclination of the steel backing plate is small, the model soil settlement is small, and the deformation of the excavation hole is not obvious . When the excavation of hole B is completed, the net spacing of the three holes is reduced to 50mm, the inclination of the steel backing plate gradually increases, and the stress around the hole increases, resulting in the excavation hole and the soil between two adjacent excavation holes. The strips are severely deformed, such as cracks and staggered damage in the soil strips between holes A and B, as shown in Figure 31. The B soil-cutting hole was about 280mm away from the orifice, that is, a large area collapsed at the edge of the steel backing plate made of I-shaped steel, and the upper rigid backing plate of the model soil was exposed, as shown in Figure32.

Figure.31: The state of soil strips between hole A and hole B in working condition 4

Figure.32 Surface state of four soil holes B under working condition

In summary, the failure of the cut hole under the four working conditions is plastic failure. The failure of the soil excavation hole first damages the two sides of the hole, and then the upper part of the hole is destroyed immediately, and the upper structure edge is destroyed first. This is because the stress on both sides of the oval soil excavation hole is the largest under the upper load, and the failure condition is reached first.

5 Conclusion

(1) Aiming at the serious weathering of the stone statue body, the small weight, the small building area and the defects of the traditional circular soil excavation hole, the elliptical soil excavation correction method is proposed, and the comparison of the long and short axis of the oval soil excavation hole is analyzed. The impact of stability. The results show that as the ratio of the long and short axis of the elliptical digging hole increases, the digging hole changes from a stable state to an unstable state. Especially when the ratio of the long and short axis of the excavation hole is equal to 1, the excavation hole is the most stable at this time, which shows that the circular excavation hole is more stable than the elliptical

excavation hole. Therefore, when the upper load is small, the elliptical digging hole is more prone to instability and deformation, and it is more likely to cause the settlement of the side foundation of the digging. It can effectively solve the problem of "correcting without tilting" when the upper load of the traditional round digging hole is small. problem.

(2) Use the finite element software to analyze the influence of different elliptical digging hole span-to-height ratio, hole buried depth and hole spacing on the elliptical digging soil tilt correction effect. The analysis results show that when the depth of the digging hole, the distance between the holes and the depth of the digging hole remain unchanged, the settlement difference between the digging side and the non-digging side increases as the span-to-height ratio of the digging hole increases; when the digging hole span-to-height ratio increases , When the hole spacing and hole depth remain unchanged, the shallower the depth of the digging hole, the greater the settlement difference between the digging side and the non-digging side; when the digging hole span-to-height ratio, burial depth and hole depth remain unchanged, the digging hole The settlement difference between the side and the non-excavated side decreases with the increase of the hole spacing.

(3) Through the analysis of the change law of the settlement of the superstructure of the model soil, it is found that under the four working conditions, the settlement of the superstructure changes rapidly at the beginning, then enters a slow growth stage, and finally is gradually in a stable state. Among them, the settlement change of the superstructure in working condition 1 and working condition 2 mainly occurs within 4h to 5h after the end of the soil excavation work; the settlement of the superstructure in working condition 3 and working condition 4 increases in a quadratic function in the first 18.5h, and the change is slow in the later period. Gradually stabilized.

(4) Through the analysis of the deformation of the digging hole, it can be known that the failure of the digging hole under the four working conditions is plastic failure. The damage of the earth-cut hole is firstly damaged on both sides of the hole, and then the upper part of the hole is destroyed immediately, and the upper structure edge is destroyed first. This is because under the upper load, the stress on both sides of the elliptical excavation hole is the largest and first reaches the failure condition.

References

[1]Zhang Yunhe, Zhang Jiaqi, Luo Kailu. The protection status of Qianling stone statues and thoughts on the protection plan[J]. Cultural Relics Appreciation, 2020, (07): 98-99.

[2]Terracina, Fernando. Foundations of the Tower of Pisa[J]. Géotechnique, 1956, 12(4):336-339.

[3]Tugaenko N F, Matus Y V, Sinyavskii S D. Rectifying tilt of 16-story residential building[J]. Soil Mechanics & Foundation Engineering, 1979, 16(2):63-65.

[4]Green A G. General Biharmonic Analysis for a Plate Containing Circularcavitys.

Proceedings of the Royal Society of London. Series A,Mathematical and Physical Sciences, 1940, 176(964):121~139.

[5] Liu Zude. Fifteen years of correction and anti-tilt engineering [J]. Geotechnical Foundation. 2006, (6): 83-87.

[6]Qin Shanglin, Chen Shanxiong, Wang Ren. Application of horizontal excavation method and grouting technology in building deviation correction[J]. Rock and Soil Mechanics, 2002, 23(s1): 88-90.

[7]Zhu Yanpeng, Wang Xiuli, Zhou Yong. Theoretical analysis and practice of rectification and reinforcement of inclined buildings in collapsible loess area with expansion method[J]. Chinese Journal of Rock Mechanics and Engineering, 2005, 24(015): 2786-2794.

[8]Zhang Xuqiang. Research on simulation analysis and reinforcement method of the whole process of immersion correction of ancient masonry tower[D]. [Master's thesis]. Xi'an: Xi'an University of Architecture and Technology, 2008.

[9]Cheng Xiaowei, Wang Zhen, Zhang Xiaobing. Research on the reasons for tilting of a high-rise residential building and its tilt correction and reinforcement technology[J]. Chinese Journal of Geotechnical Engineering, 2012(4):756-761.

[10]Sun Jianping, Wei Huanwei, Xu Xiangdong. Research on Theory and Practice of Digging Soil to Rectify Inclination[J]. Journal of Shandong Jianping University, 2008, (02):174-178.

[11]Wang Guifang. Tunnel Calculation Common Deformation Theory[M]. Chengdu University of Science and Technology Press, 1992.

[12] Zhao Minghua. Soil Mechanics and Basic Engineering [M]. Wuhan University of Technology Press, 2009.

[13] Li Bin, Fan Qiuyan, Qin Fengrong. Stability analysis of cave roof in karst area[J]. Chinese Journal of Rock Mechanics and Engineering, 2002, 21(4): 532-536.

Corresponding author:Qingwen Ma

Email: Mqw2008@zzu.edu.cn

TEL: +86 18539982987

Address: School of Water Conservancy Science and Engineering, Zhengzhou University, 100 Science Avenue, Zhengzhou, Henan Province P.R. China

Zip code: 450001

Figures

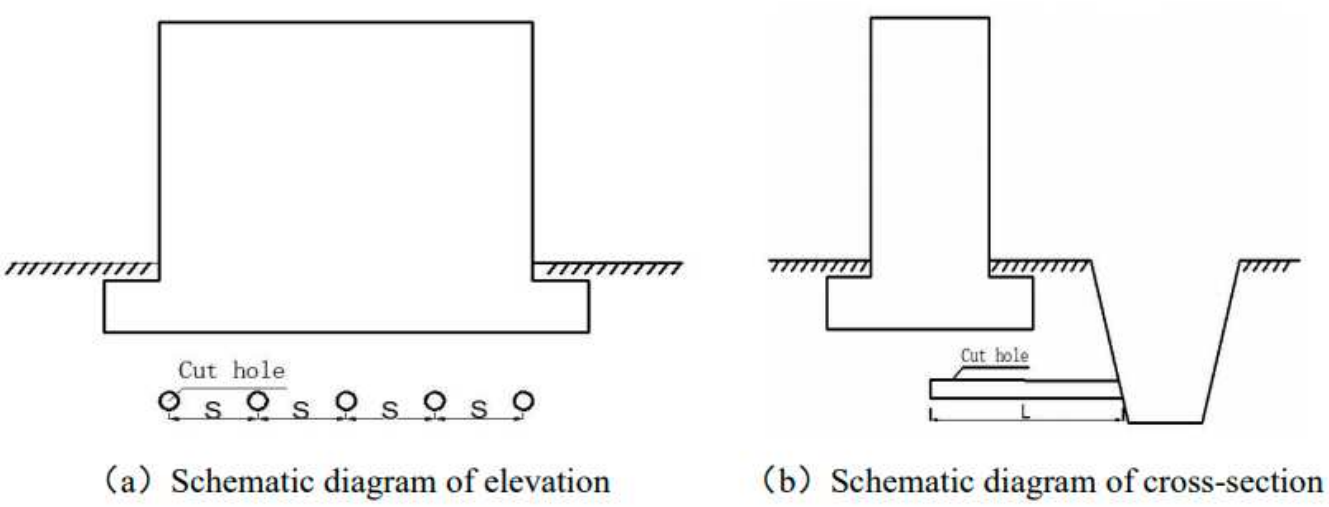

（a）Schematic diagram of elevation　　（b）Schematic diagram of cross-section

Figure 1

Please see the Manuscript PDF file for the complete figure caption

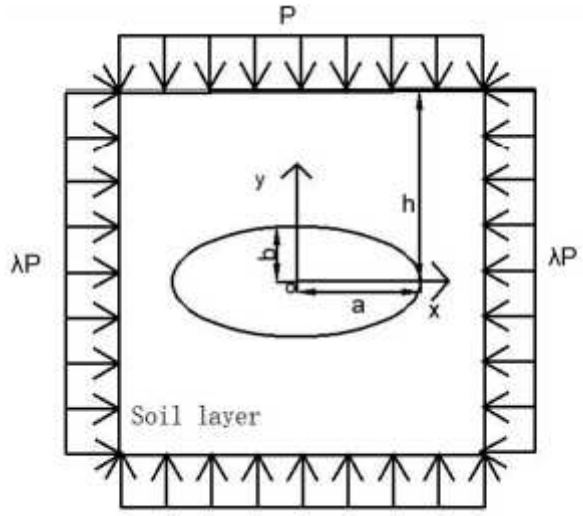

Figure 2

Please see the Manuscript PDF file for the complete figure caption

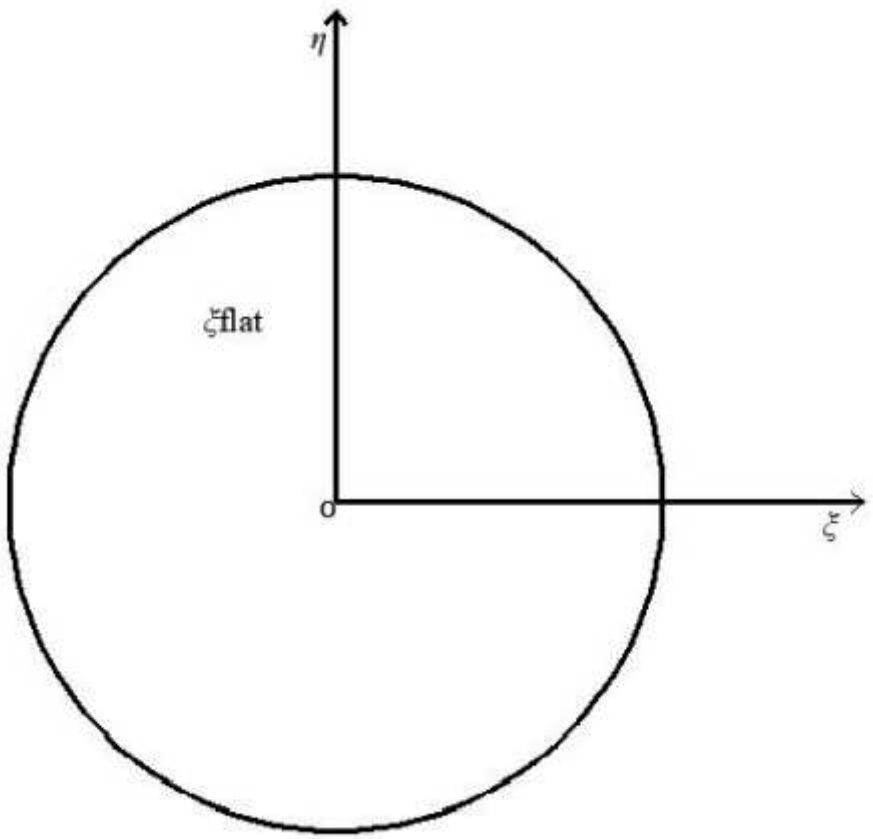

Figure 3

Please see the Manuscript PDF file for the complete figure caption

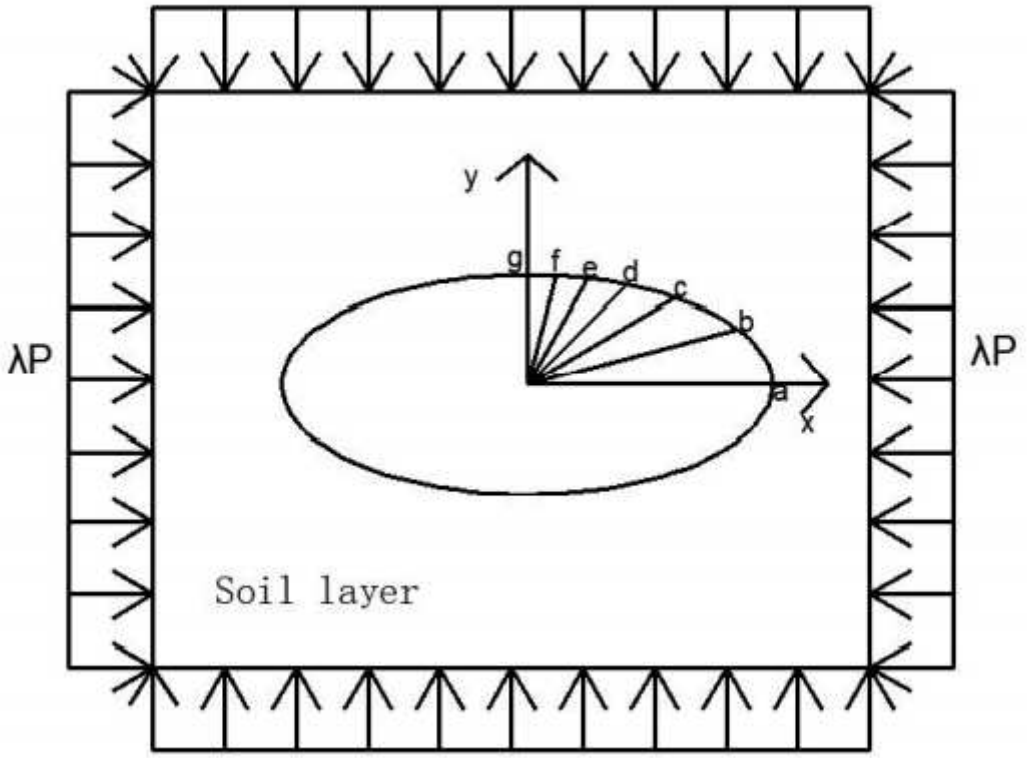

Figure 4

Please see the Manuscript PDF file for the complete figure caption

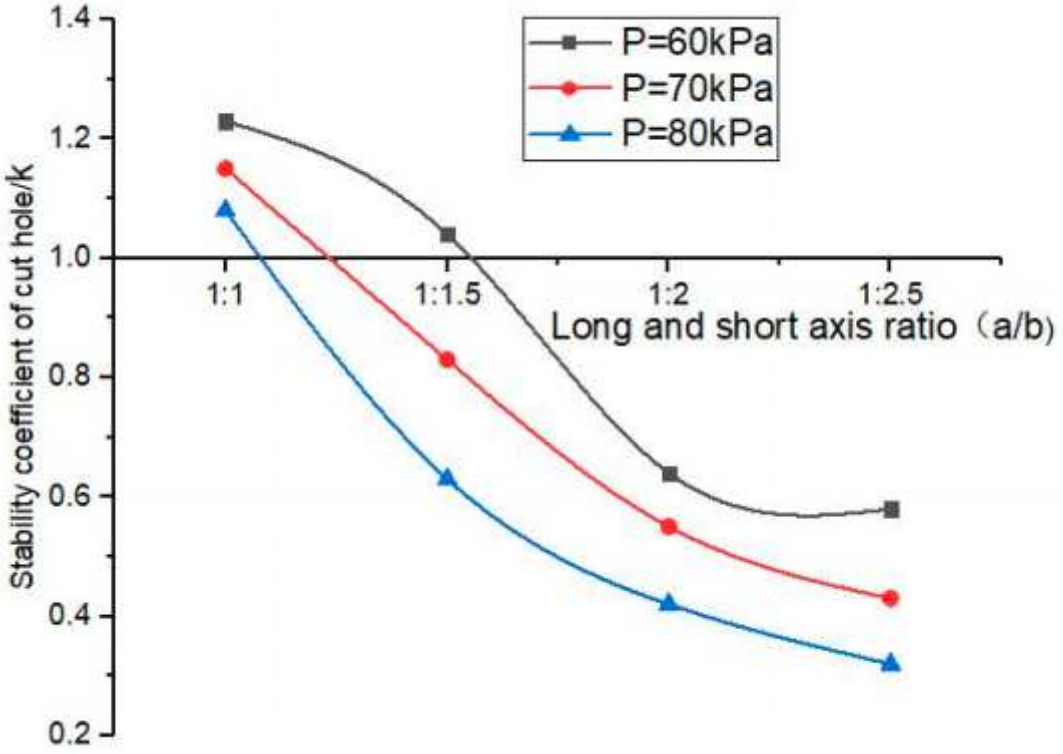

Figure 5

Please see the Manuscript PDF file for the complete figure caption

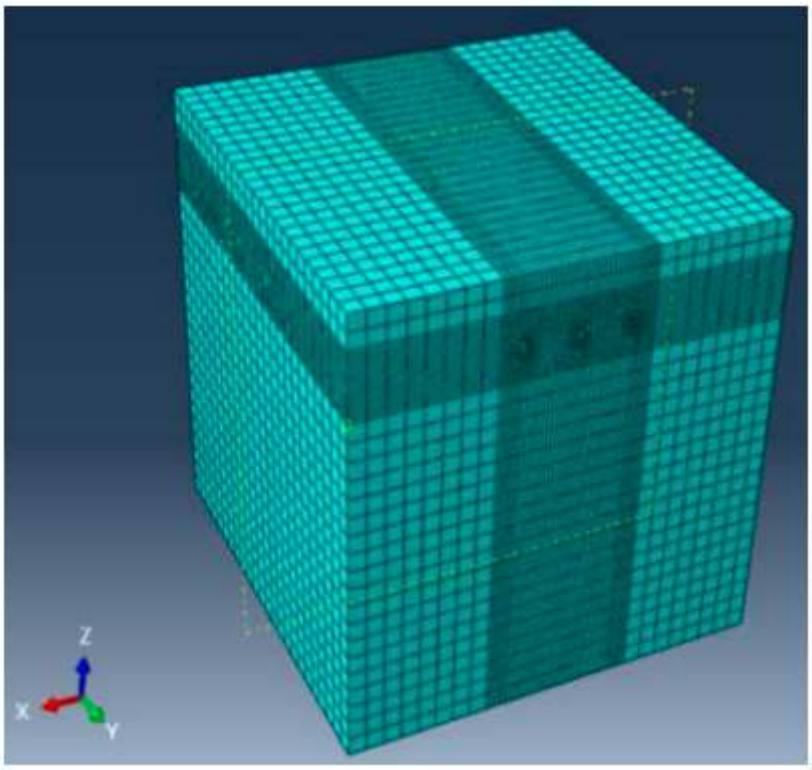

Figure 6

Please see the Manuscript PDF file for the complete figure caption

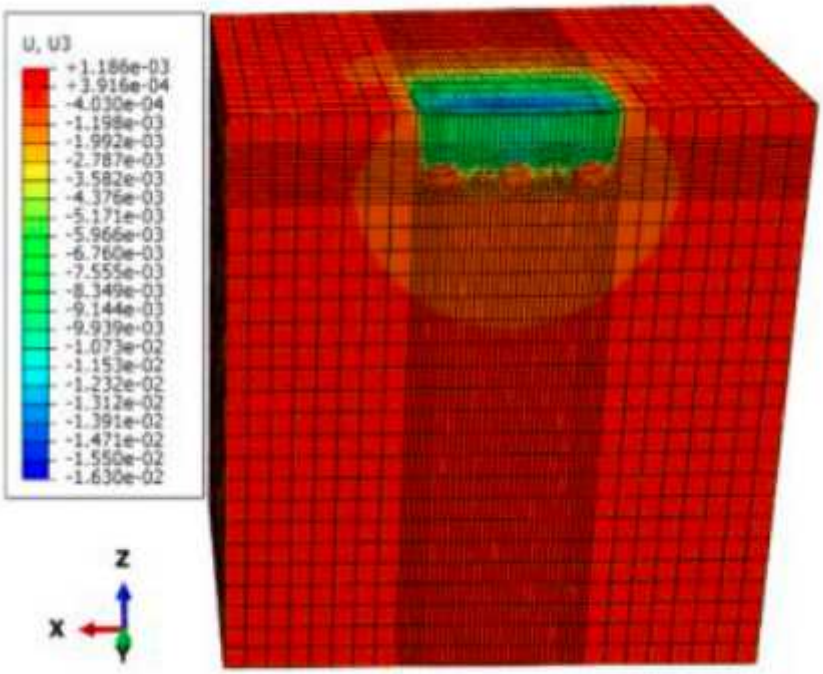

Figure 7

Please see the Manuscript PDF file for the complete figure caption

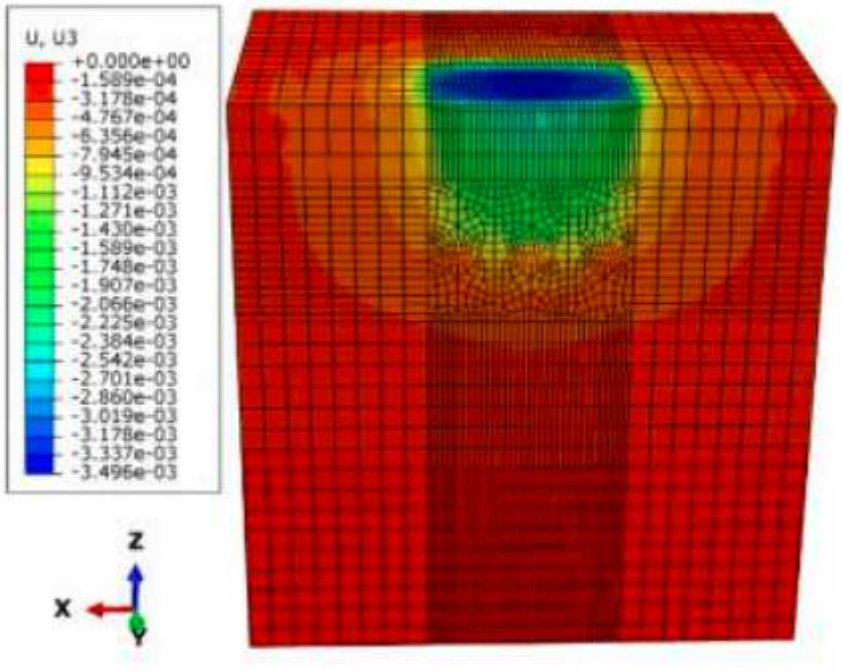

Figure 8

Please see the Manuscript PDF file for the complete figure caption

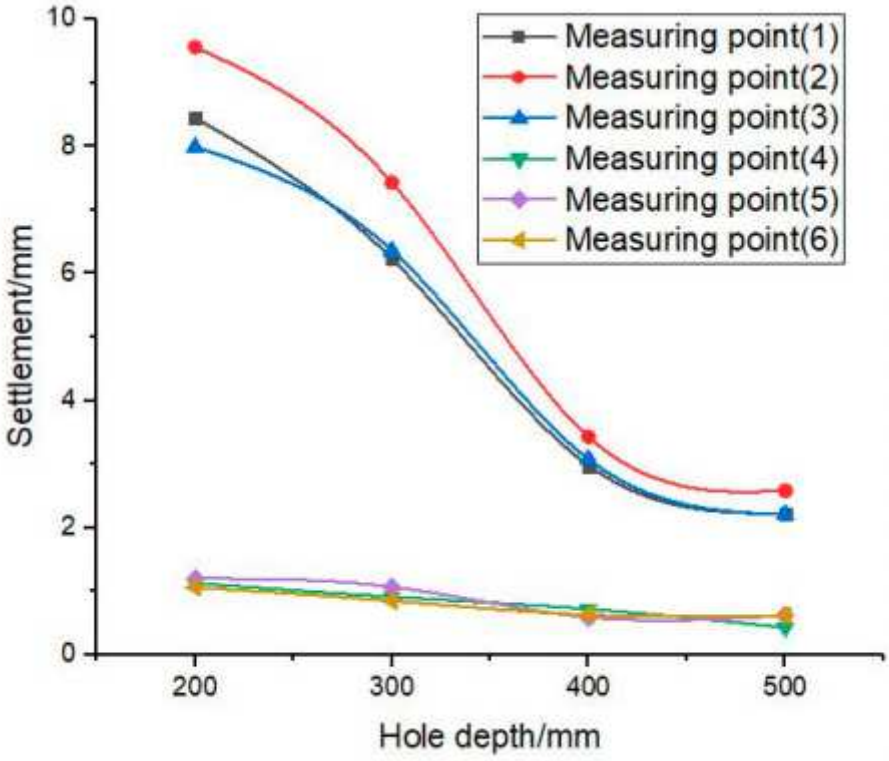

Figure 9

Please see the Manuscript PDF file for the complete figure caption

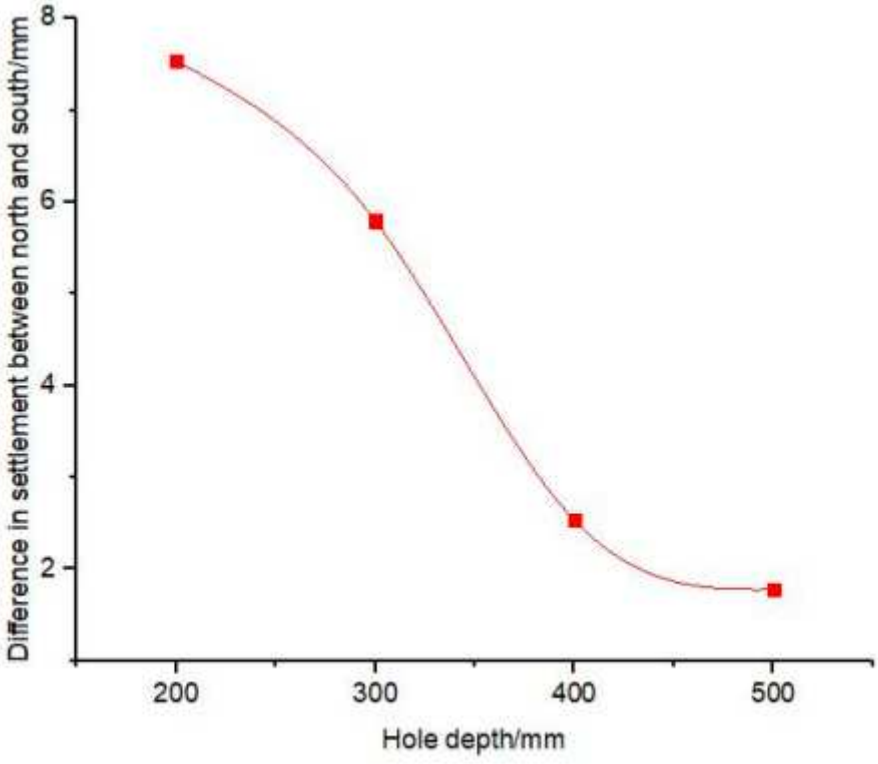

Figure 10

Please see the Manuscript PDF file for the complete figure caption

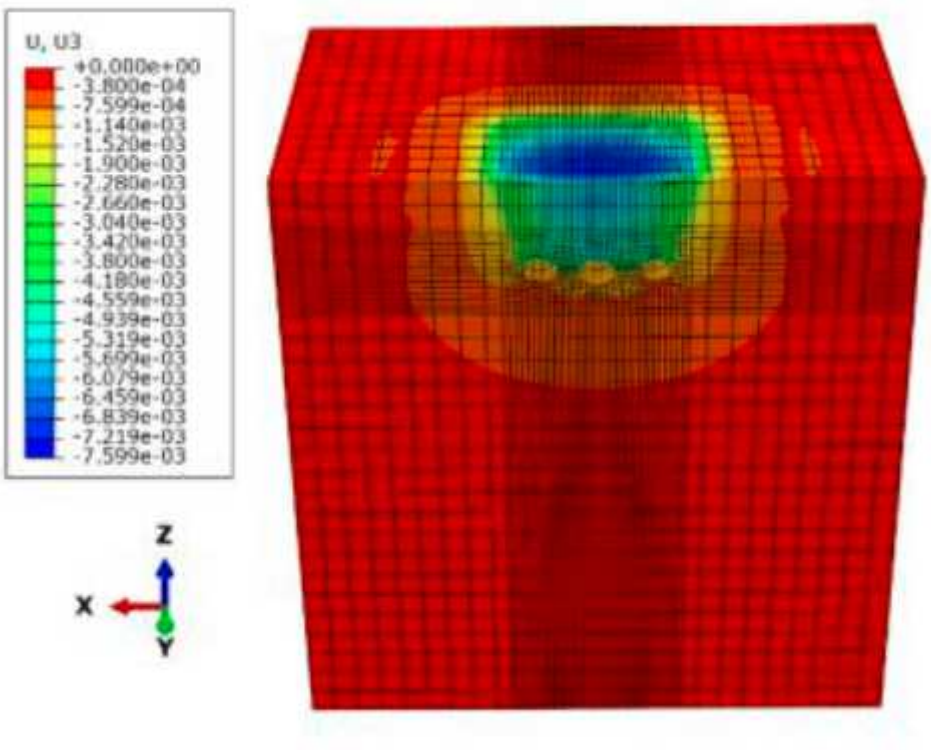

Figure 11

Please see the Manuscript PDF file for the complete figure caption

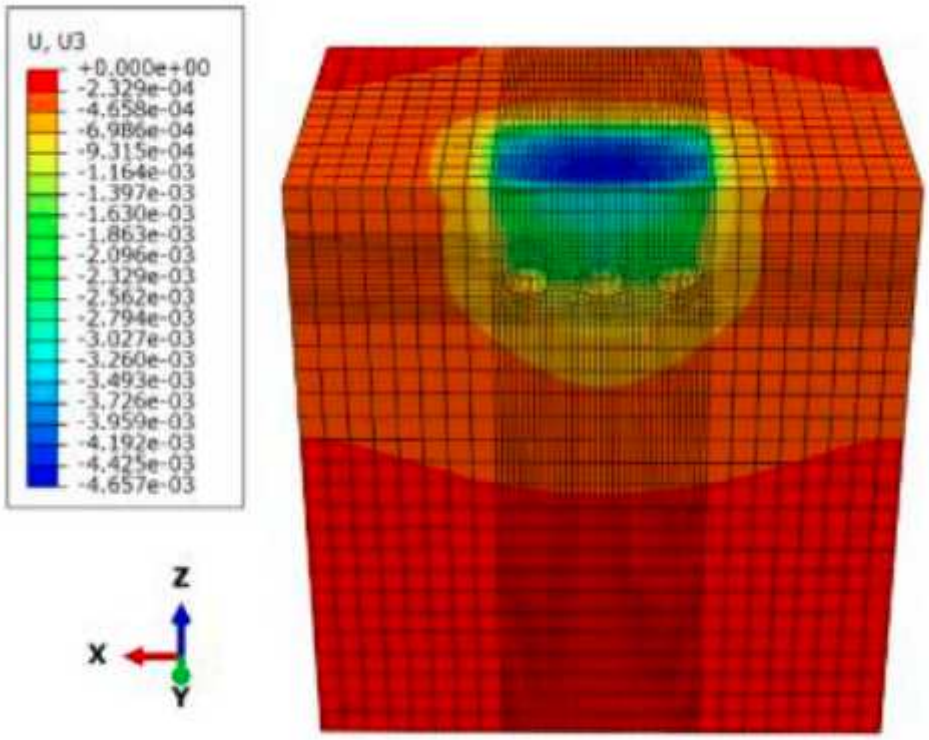

Figure 12

Please see the Manuscript PDF file for the complete figure caption

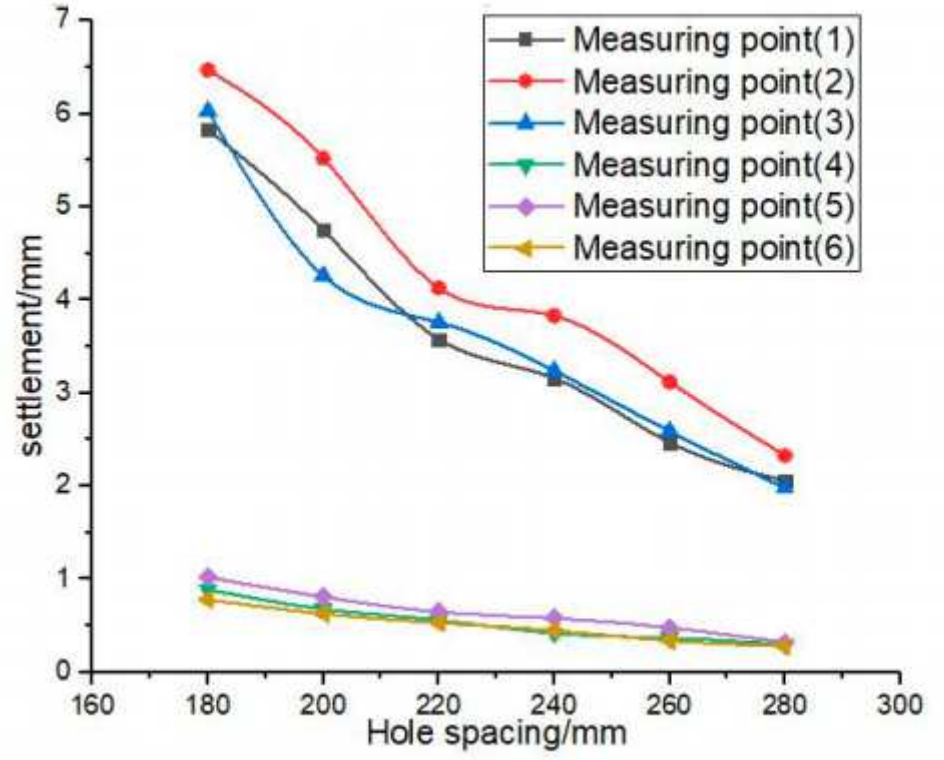

Figure 13

Please see the Manuscript PDF file for the complete figure caption

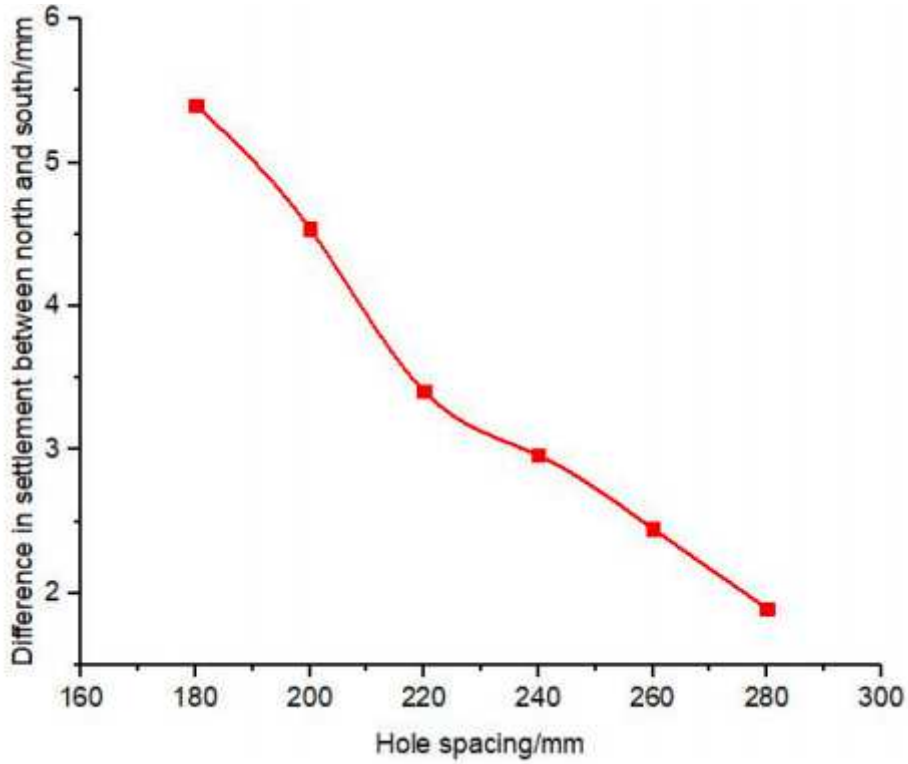

Figure 14

Please see the Manuscript PDF file for the complete figure caption

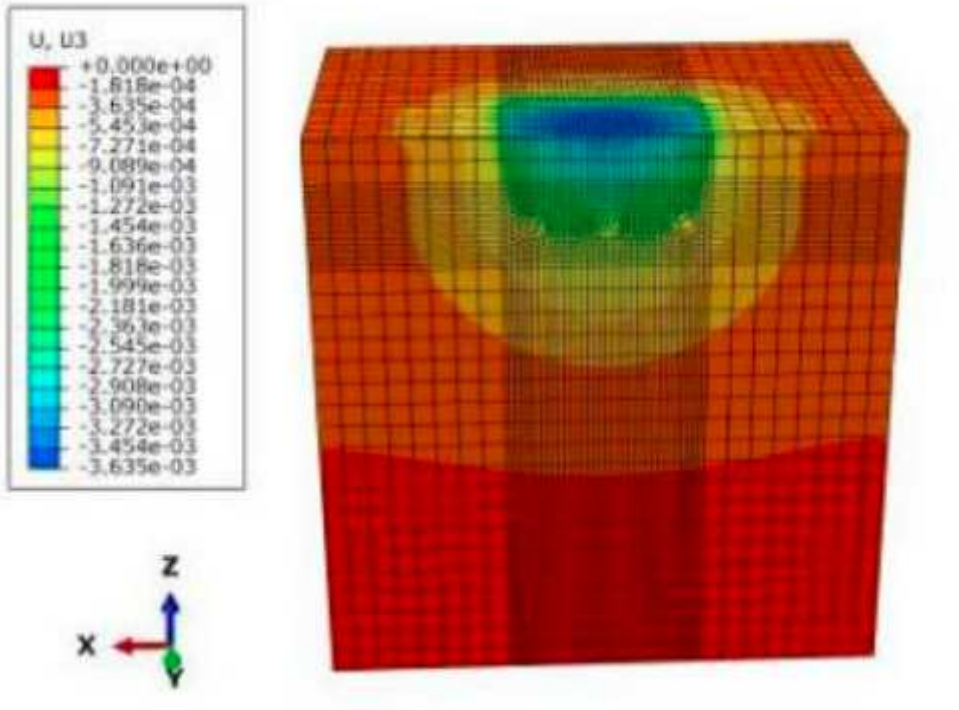

Figure 15

Please see the Manuscript PDF file for the complete figure caption

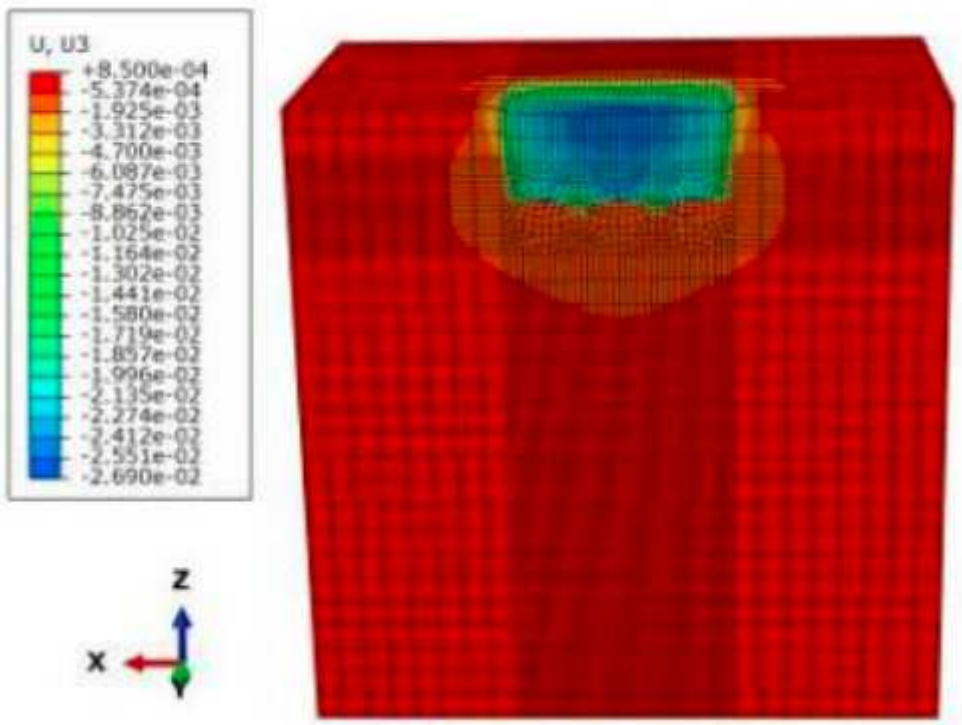

Figure 16

Please see the Manuscript PDF file for the complete figure caption

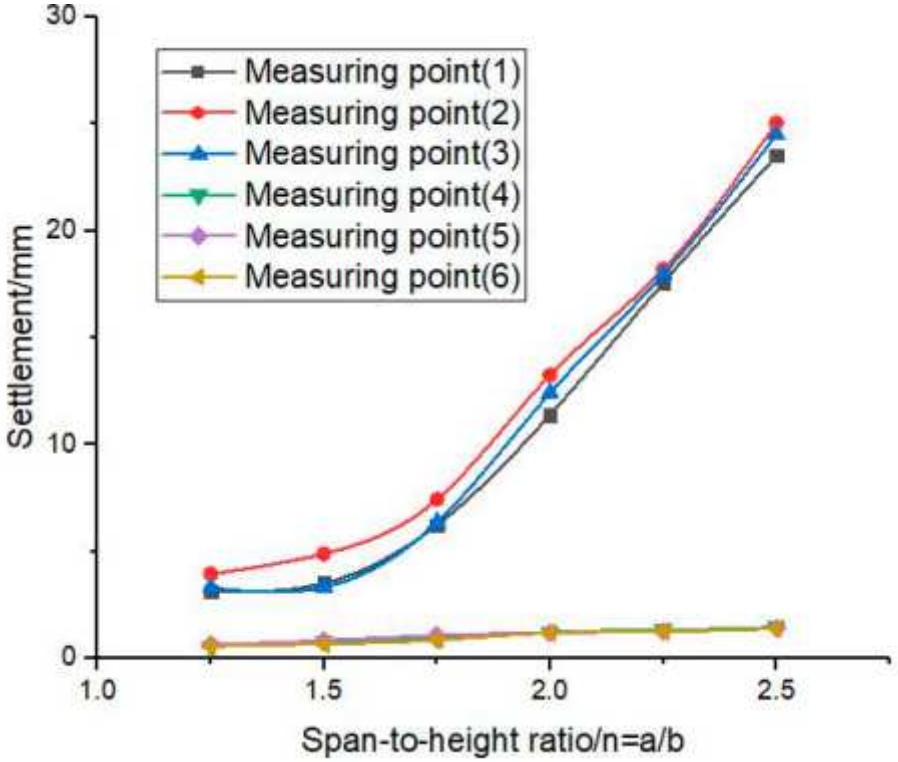

Figure 17

Please see the Manuscript PDF file for the complete figure caption

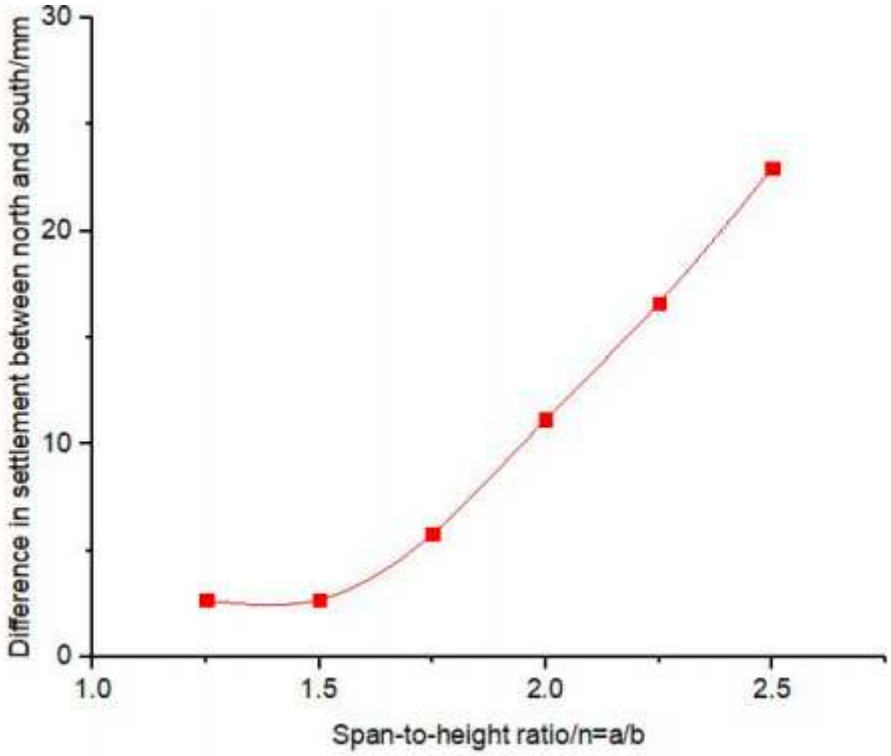

Figure 18

Please see the Manuscript PDF file for the complete figure caption

(a) Model box

(b) The box is filled with soil

Figure 19

Please see the Manuscript PDF file for the complete figure caption

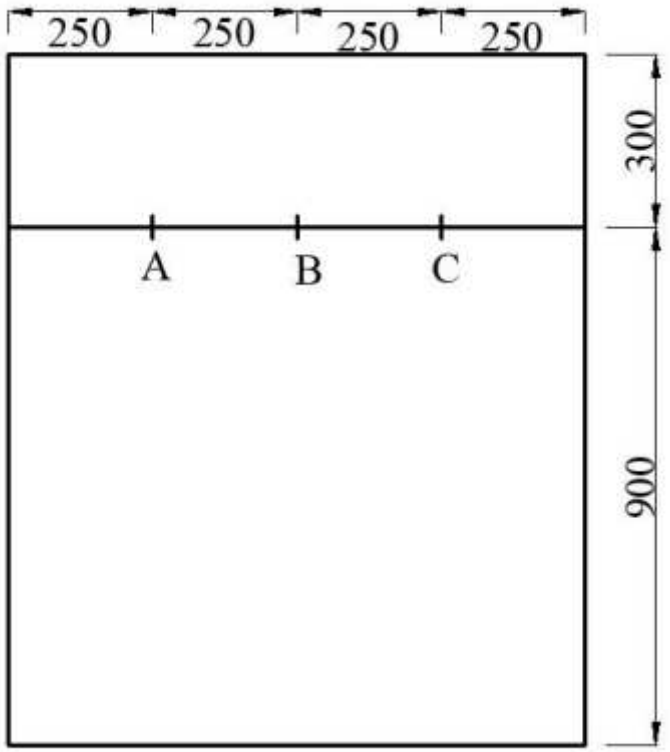

Figure 20

Please see the Manuscript PDF file for the complete figure caption

Figure 21

Please see the Manuscript PDF file for the complete figure caption

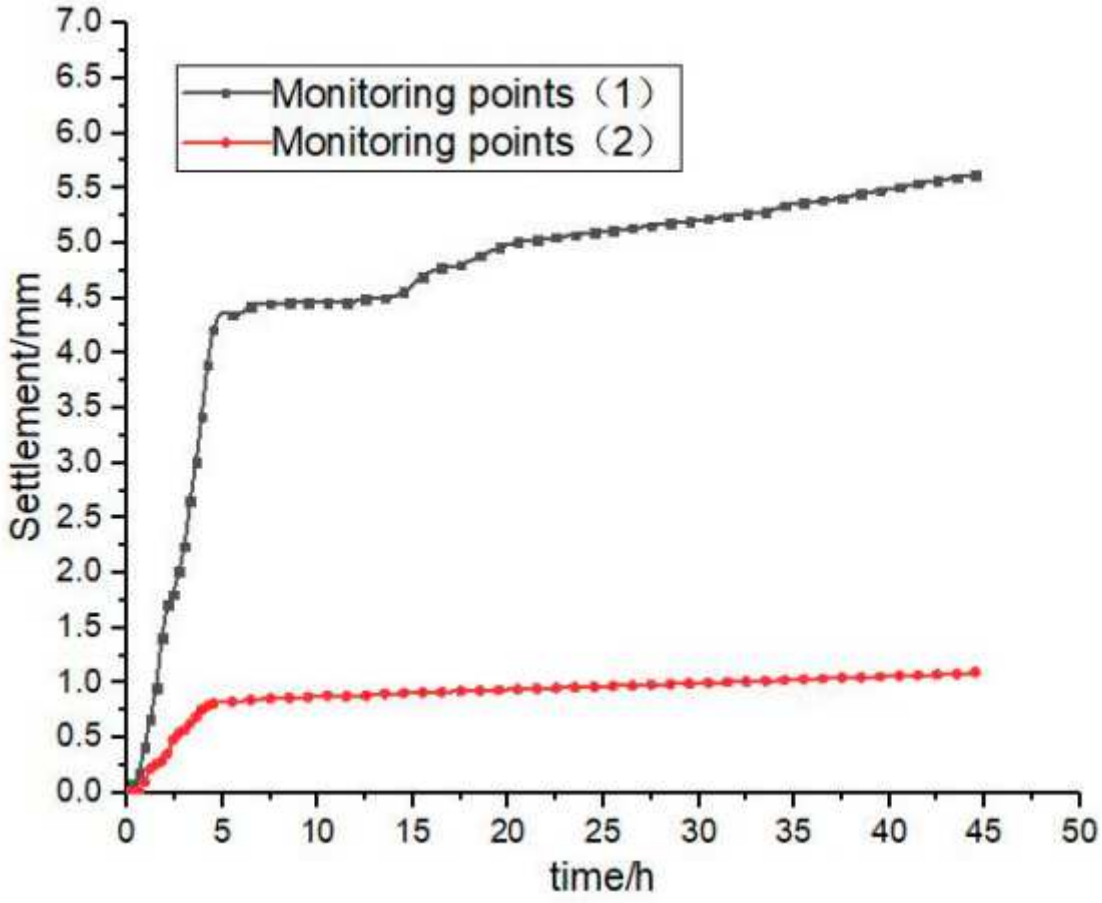

Figure 22

Please see the Manuscript PDF file for the complete figure caption

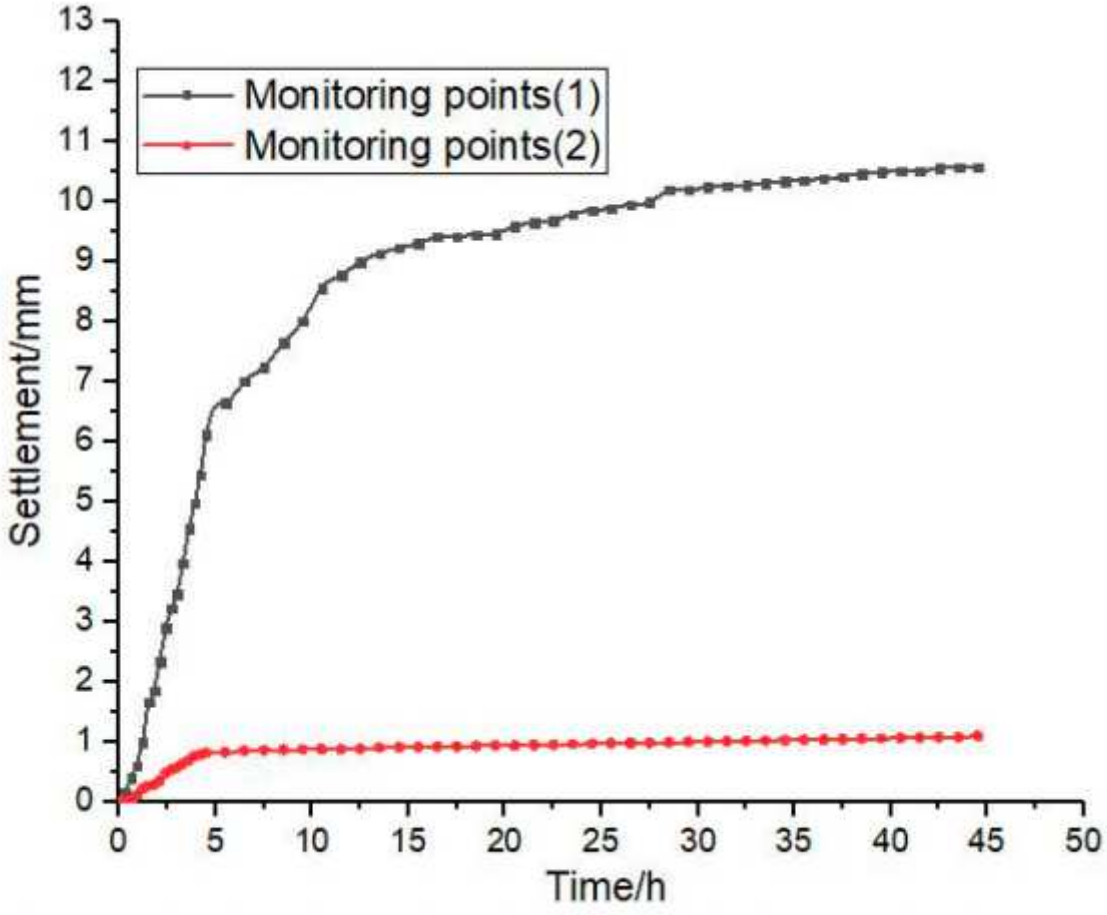

Figure 23

Please see the Manuscript PDF file for the complete figure caption

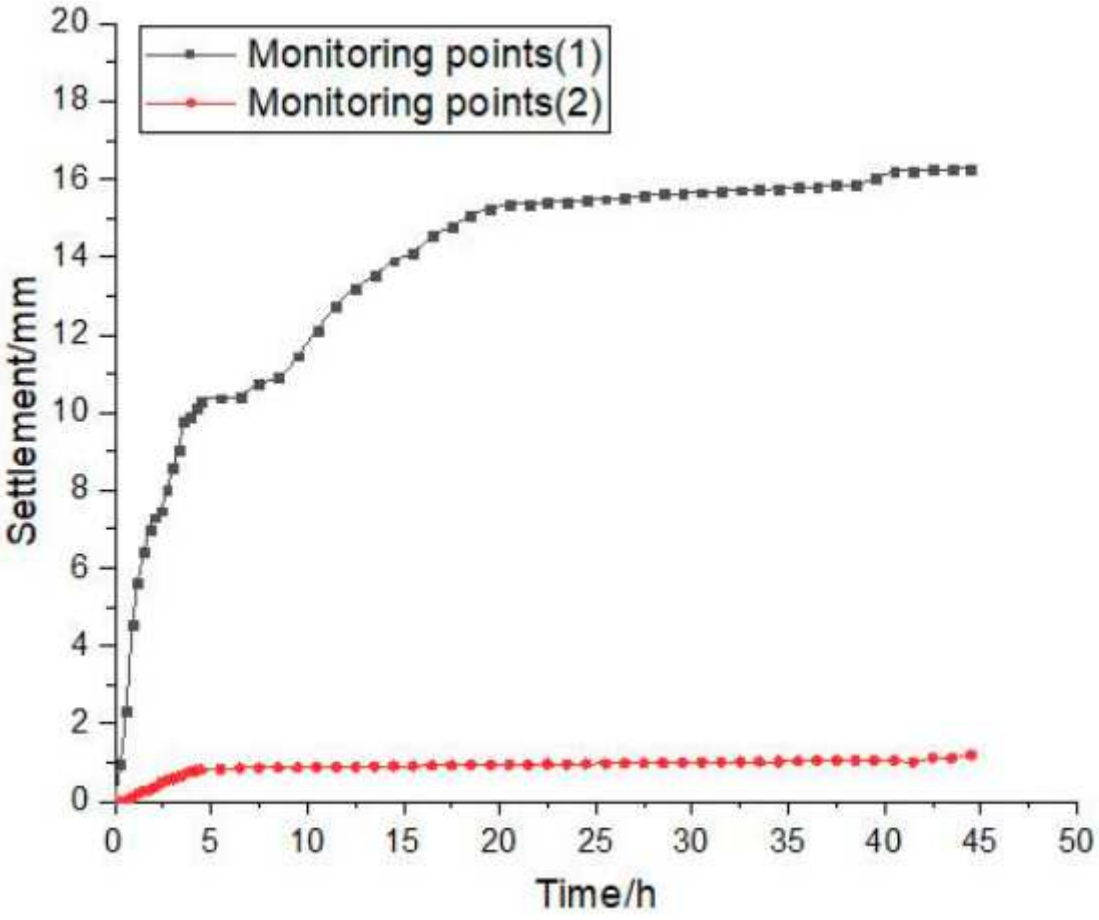

Figure 24

Please see the Manuscript PDF file for the complete figure caption

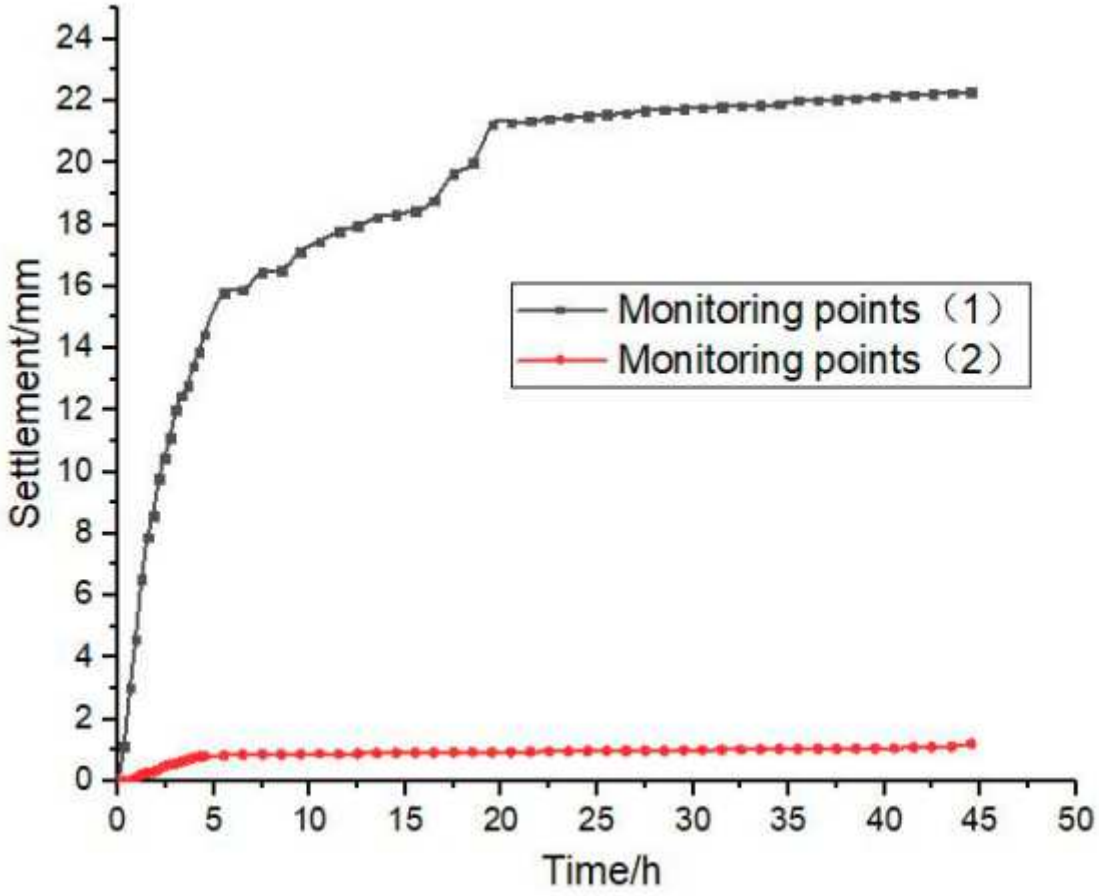

Figure 25

Please see the Manuscript PDF file for the complete figure caption

Figure 26

Please see the Manuscript PDF file for the complete figure caption

Figure 27

Please see the Manuscript PDF file for the complete figure caption

Figure 28

Please see the Manuscript PDF file for the complete figure caption

Figure 29

Please see the Manuscript PDF file for the complete figure caption

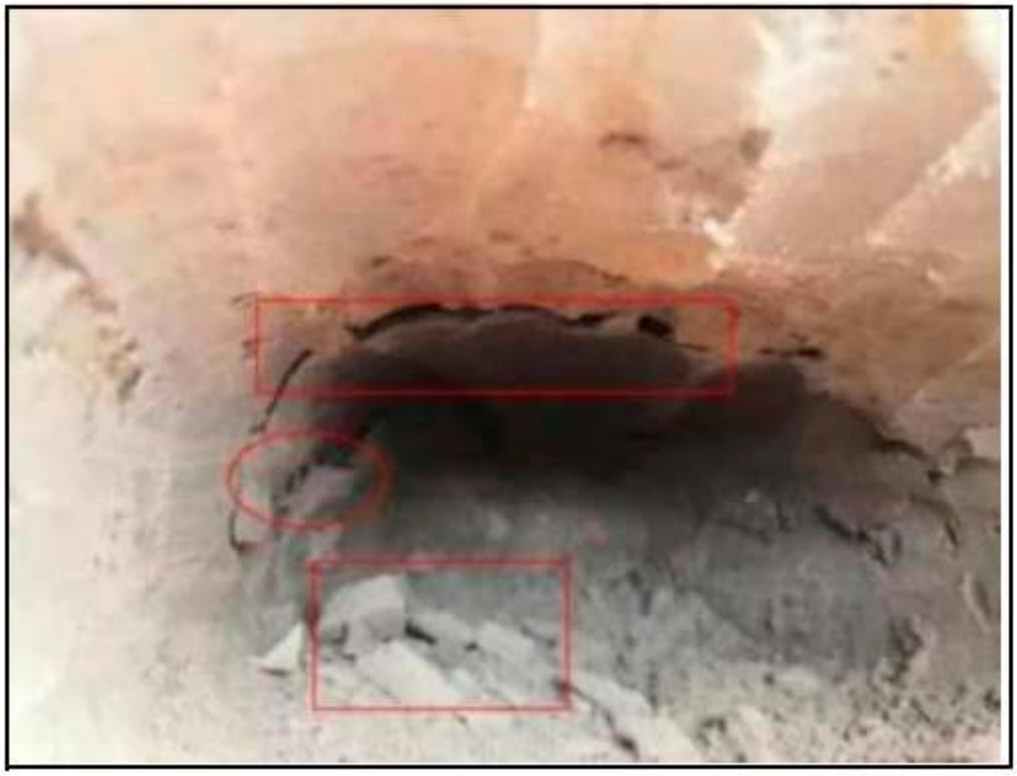

Figure 30

Please see the Manuscript PDF file for the complete figure caption

Figure 31

Please see the Manuscript PDF file for the complete figure caption

Figure 32

Please see the Manuscript PDF file for the complete figure caption